CONTRIBUTION OF THE TWO RECTIFIERS RECONFIGURATION TO FAULT TOLERANCE CONNECTED TO THE GRID NETWORK TO FEED THE GMAW THROUGH PROCESSOR-IN-THE-LOOP

Omar Fethi Benaouda[1*] – Badreddine Babes[1] – Mohamed Bouchakour[2] –Azzedine Bendiabdellah[3]

[1]Research Center in Industrial Technologies CRTI, P.O.Box 64, Cheraga 16014, Algiers, Algeria.
[2]Department of physics, Faculty of exact sciences and informatics, PCME laboratory, University of Djelfa, Algeria.
[3]Diagnostic Group, LDEE laboratory, Faculty of Electrical Engineering, University of Sciences and Technology of Oran MB, BP 1505 El-M'naouer, Oran 31000, Algeria.

ARTICLE INFO

***Article history*:**
Received: 12.10.2021.
Received in revised form: 08.05.2023
Accepted: 10.05.2023.

Keywords:
Grid network
Rectifiers Reconfiguration
Gas Metal Arc Welding
Open-circuit fault
Thyristor
Diagnosis
Processor-in-the-loop

DOI: https://doi.org/10.30765/er.1884

Abstract:

This study aims to propose a new diagnosis technique based on the Park's vector and the polar coordinates of electric currents for the detection and location of open-circuit faults (OC) at the level of two rectifiers connected to the grid network to feed the Gas Metal Arc Welding process (GMAW). This diagnosis technique allows the early location of faulty switches (Thyristors) to overcome the negative effect of faulty rectifiers on welding current, welding voltage, and droplet diameter. For that, the reconfigurable rectifiers have been integrated to accomplish the welding process. The proposed diagnosis technique is applied to reconfigurable rectifiers connected to the GMAW system through numerical simulations using MATLAB/Simulink and real-time processor-in-the-loop (PIL) implementation via DSpace ds 1103 card. The simulation and PIL experimental results show similar trends and great success of the diagnosis technique and the two rectifiers reconfiguration for overcoming the open circuit faults and obtaining high welding quality while maintaining the work-piece and avoiding the distortions caused by the faulty rectifiers, which affecting the grid network and on the GMAW system at the same time.

1 Introduction

Welding is currently considered the most important process for joining metallic structures. Among many types of welding processes, the Gas Metal Arc Welding (GMAW) process meets several of today's requests including high productivity, good quality, and low cost [1]. It is often used in the semi-automatic form but can be relatively easily automated [2, 3].

In most arc welding applications, the rectifier is used as a source of arc current to feed the GMAW system. The rectifier uses power switches based on Thyristors to obtain acceptable frequency. A two-level three-phase rectifier produces the high-power and current in industrial welding. If two rectifiers are connected in series with each other, they will have better power ability compared with three-level three-phase rectifiers; in addition, they give high frequency. This topology can improve the power quality and enlarge the power rating compared to the conventional 2-level topology [4], furthermore, it offers the possibility of reducing voltage stress applied on the semi-conductor, lower harmonic components, and controllable output DC voltage. These advantages are not occurring except by providing many active devices (semi-conductor), therefore, the higher the number of semiconductors connected in series in rectifiers, the higher the possibility of incidence in the fault [5].

*Corresponding author
E-mail address: benaouda.omar@gmail.com

Generally, in systems containing rectifiers, most of the faults of an electrical system occur in the rectifier and/or its control. Inside the rectifier, most of the critical and frequent faults are related to switching control [6].
According to the point of reliability in the arc welding system, the GMAW is fed by two rectifiers which are more susceptible to faults in their switches (Thyristors).
To detect and locate the faulty switches, the diagnosis is the most appropriate technique because of the reliability improvement and planned maintenance assurance.
On the whole, the majority of faults can be classified as open-circuit and short-circuit [7].
In the last decade, some diagnosis techniques of open-circuit fault in the rectifier have been developed by Mendes, Abramik, and Peuget et al [8,9].
Bin Lu is considered among some researchers interested in studying the behavior of the inverter before and after fault inducing [10,11], on the contrary, there are few researchers interested in the diagnosis of rectifiers.
To detect and locate faults, there are several techniques, they are often relied on the mean values of currents under the Park d-q vector, and examined by the threshold band to distinguish between the switches' open circuit faults [12,13].
Application of diagnosis technique based on the Park's vector and the polar coordinates is considered a new tool applied in the arc welding field.
Many researchers concentrate on the concepts of fault tolerance to overcome faults in the system and guarantee acceptable performance through changing its structure and/or control of the converter [14]. There are many ways of converter reconfiguration topologies [15], based on adding some basic topology devices [16] such as:

- Addition of a fourth leg that can be used after isolating the faulty leg (the redundancy phase design method)
- Isolation of the faulty leg with changing the control of the healthy switches.

This investigation suggests a new diagnostic technique based on the Park's vector and the polar coordinates for the open circuit fault at the Thyristors in the fault-tolerant rectifiers which are connected to GMAW, the two rectifiers are fed from the grid network.
Firstly, a global system modeling includes part of the GMAW and the other represented in the two rectifiers are connected to the grid network, this set is put in the healthy state i.e. without open-circuit fault of the switches (Thyristors).
Secondly, an open circuit fault of the Thyristor switches is induced in the two rectifiers.
Thirdly, the faults diagnostic technique based on Park's vector and polar coordinates is used to detect and locate the faults and subsequently comparing between the graphical polar coordinates of the faults, this technique is applied on two reconfigurable rectifiers.
Finally, study the importance of integrating fault-tolerant rectifiers and discuss the influences of the open circuit faults on the GMAW system. The numerical simulations and real-time processor-in-the-loop (PIL) validation have been implemented to confirm the performance of the proposed diagnostic technique on the grid network -GMAW system.

2 Modeling of a Gas Metal Arc Welding (GMAW)

The static equilibrium theory postulates that the detachment of the electrode drop occurs when the static forces of detachment (gravity F_g , electromagnetic forces F_{em}, and the plasma drag forces F_d) are superior to the static forces of attachment (surface tension force F_γ). In this theory, the drop is considered as a sphere suspended at the electrode in a liquid metal [17].
Based on the modified force balance model (MFBM), the resultant force affecting the droplet is as follows [18]:

$$F_T = F_g + F_{em} + F_d + F_{mf} \quad (1)$$

Where F_{mf} the momentum flux force. The gravity force F_g depends solely on the mass of molten metal and is a detachment force when the weld is flat:

detachment force when the weld is flat:

$$F_g = \frac{4}{3}\pi r_d^3 \rho_d g \tag{2}$$

With r_d is the radius of the drop, ρ_d is the density of the drop and g is the gravity constant. The electromagnetic force on a drop results from the convergence or divergence of the current lines in the drop, it is given by the Lorentz law:

$$F_{em} = \vec{J} \times \vec{B} \tag{3}$$

Where $\vec{J}$ is the current density, and $\vec{B}$ is the magnetic induction.
The total magnetic force can be obtained by integrating equation (3) on the conductive surface of the drop. Assuming that the current surface density is uniform, Amson [19] obtained:

$$F_{em} = \frac{\mu_0 I_a^2}{4\pi}\left[\ln\left(\frac{r_d \sin\theta}{r_e}\right) - \frac{1}{4} - \frac{1}{1-\cos\theta} + \frac{2}{(1-\cos\theta)^2}\ln\left(\frac{2}{1+\cos\theta}\right)\right] \tag{4}$$

Where I_a is the welding current and μ_0 is the permeability of the free space, θ is the angle of the arc-covered area, and r_e is the radius of the electrode.
The plasma drag force F_d can be calculated by considering the drag force experienced by a sphere immersed in a fluid having a uniform velocity field:

$$F_d = \frac{1}{2}\left(c_d A_d \rho_p v_p^2\right) \tag{5}$$

Where c_d is the drag coefficient, ρ_P is the density of the plasma, v_P is the shielding gas velocity, and A_d is the area of droplet hit by the shielding gas:

$$A_d = \pi\left(r_d^2 - r_e^2\right) \tag{6}$$

The momentum flux F_{mf} is determined as follows [20]:

$$F_{mf} = \frac{\mu_0 I_a^2}{4\pi}\left[\frac{1}{\alpha^2} - \left(1 - \sqrt{1 - \frac{1}{\alpha^2}}\right)^2\right] \tag{7}$$

Where α is defined as r_d/r_e (r_e is the weld wire radius and r_d is droplet radius).
The surface tension force F_γ that holds the drop to the electrode is given as follows:

$$F_\gamma = 2\pi r_e \gamma \tag{8}$$

Where γ is the surface tension coefficient of the liquid metal. We can determine the diameter of the droplet before the detachment D_{dbd} by equating the total static forces of detachment F_T and the detaching preventive force F_γ :

$$F_T = F_\gamma \rightarrow F_{em} = F_\gamma - F_g - F_d - F_{mf} \tag{9}$$

By substituting for F_{em} from (4) and (9) can be written as

$$\frac{\mu_0 I_a^2}{4\pi}\left[\ln\left(\frac{D_{dbd}\sin\theta}{r_e}\right) - \frac{1}{4} - \frac{1}{1-\cos\theta} + \frac{2}{(1-\cos\theta)^2}\ln\left(\frac{2}{1+\cos\theta}\right)\right] = F_\gamma - F_g - F_d - F_{mf} \tag{10}$$

Finally, the detaching droplet diameter size is obtained by the following relation [20]:

$$D_{dbd} = \frac{2r_e}{\sin\theta} e^{\left(\frac{F_\gamma - F_g - F_d - F_{mf}}{\frac{\mu_0 I_a^2}{4\pi}} - k_1 \right)} \tag{11}$$

With

$$k_1 = \left[-\frac{1}{4} - \frac{1}{1-\cos\theta} + \frac{2}{(1-\cos\theta)^2} \ln\left(\frac{2}{1+\cos\theta} \right) \right] \tag{12}$$

The fifth-order nonlinear state space model in the GMAW process was introduced in [21,22]. The state variables are:

I_a = welding current;
l_s = stick out;
x_d= droplet displacement;
v_d = droplet velocity;
m_d= droplet mass;

Table 1. Parameters and some variables of GMAW process nonlinear model used in the simulation

Nomenclature	Symbol	Value (unit)
Arc resistance	R_a	0.0237 (Ω)
Arc length factor	E_a	400 (V m^{-1})
Constant charge zone	V_0	12 (V)
Shielding gas velocity	v_P	10 (m s^{-1})
Resistivity of the electrode	ρ	0.43 (Ω m^{-1})
Permeability of free space Gravity	μ_0	$4\pi\times 10^{-7}$ (H m^{-1})
Spring constant of drop	K_d	5.3 (Kg S^{-2})
Damper constant of drop	b_d	0.8×10^{-3} (Kg S^{-1})
Density of the liquid electrode material (Steel)	ρ_e	7860 (Kg m^{-3})
Total wire resistance (power supply and cable)	R_s	6.8×10^{-3} (Ω)
Total inductance (power supply and cable)	L_s	306×10^{-6} (H)
Electrode radius	r_e	0.005 (m)
Density of the plasma (Argon gas)	ρ_P	1.6 (Kg m^{-3})
Drag coefficient	C_d	0.44
Melting rate constant 1	C_1	3.3×10^{-10} (m^{-3} S^{-1} A^{-1})
Melting rate constant 2	C_2	0.78×10^{-10}
Surface tension of liquid steel (Steel)	γ	1.2 (Nm^{-1})
Angle of conducting zone with drop	θ	90 (°)
Weld wire DC motor time constant	τ_{m1}	50×10^{-3} (S)
Weld wire DC motor steady state gain	K_{m1}	1.0 (mv^{-1} S^{-1})
Torch DC motor time constant	τ_{m1}	80×10^{-3} (S)
Torch DC motor steady state gain	K_{m1}	1.0 (mv^{-1} S^{-1})

The differential equations that have been used for programming the simulator are:

$$\begin{cases} \dot{I}_a = \dfrac{1}{L_s}\left(V_{oc} - \left(R_s + \rho\left[l_s + \dfrac{1}{2}\left(\dfrac{3m_d}{4\pi\rho_e} \right)^{\frac{1}{3}} + x_d \right] + R_a \right) I_a - E_a\left(CTWD - l_s \right) - V_0 \right) \\ \dot{l}_s = S - \left(\dfrac{c_1}{\pi r_e^2} I_a + \dfrac{c_2\rho}{\pi r_e^2} I_a^2 l_s \right) \\ \dot{x}_d = v_d \\ \dot{v}_d = \dfrac{F_T - k_d x_d - b_d v_d}{m_d} \\ \dot{m}_d = \rho_e M_R \end{cases} \tag{13}$$

Where M_R is the melting rate:

$$M_R = c_1 I_a + c_2 \rho I_a^2 l_s \tag{14}$$

And S is the welding wire velocity and V_{OC} is the open-circuit voltage.
Until here, only the statics of the GMAW process before detachment is considered. To find out the dynamics of the droplet detachments, the following criterion is used [23].

$$F_T > F_\gamma \tag{15}$$

The initial conditions after each droplet detachment are set as follows:

$$\begin{cases} I_a = I_a \\ l_s = l_s \\ x_d = 0 \\ v_d = 0 \\ m_d = 0.5\, m_d \left(1 + \dfrac{1}{1 + e^{-k_2 v_d}} \right) \end{cases} \tag{16}$$

From all previous equations, it can be put Closed-loop GMAW process as shown in the figure below.

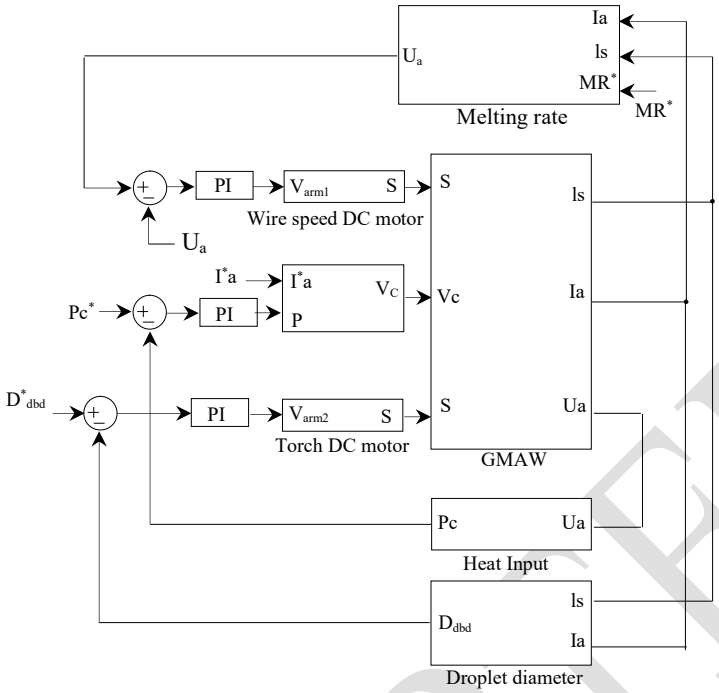

Figure 1. Closed-loop GMAW process based on the PI controllers to control melting rate, heat input, and metal droplet diameter.

3 Grid network-GMAW system

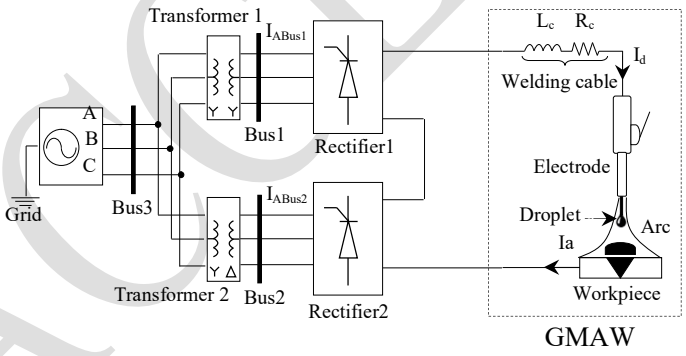

Figure 2. Grid network-GMAW system

Figure 2 shows a schematic diagram of the grid network-GMAW system. Two rectifiers connected to the GMAW system to get great value of arc current Ia.

3.1 Simulation results

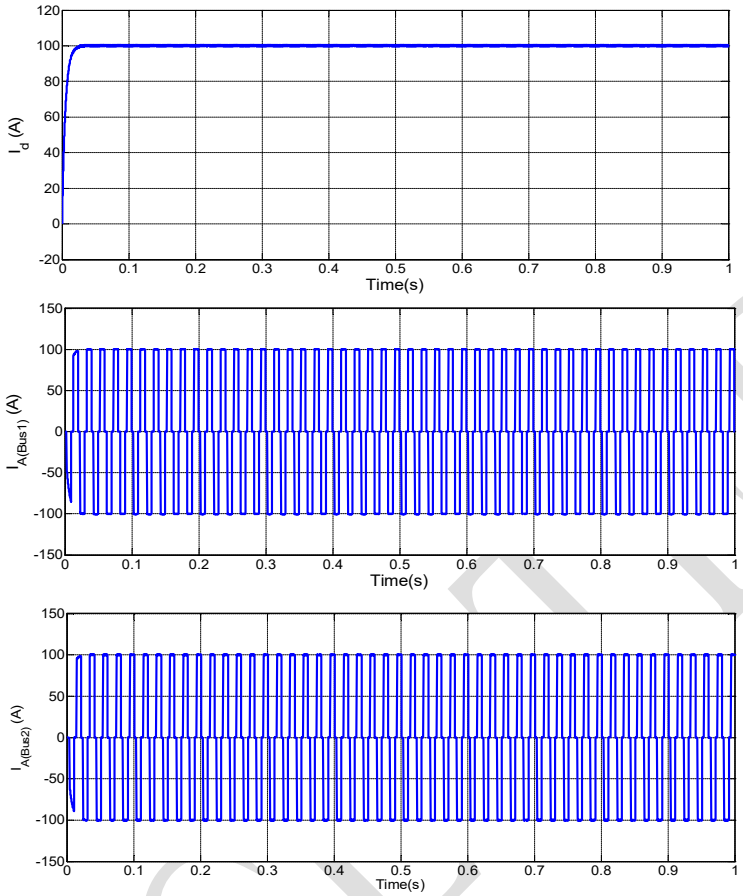

Figure 3. Simulation results of rectified current (I_d), current of the first phase of bus1(I_A(Bus1)), and current of the first phase of bus2(I_A(Bus2))

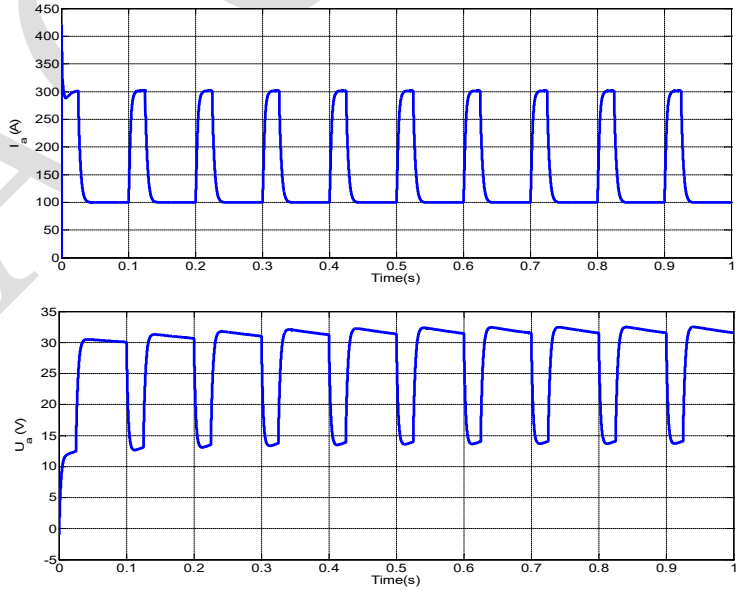

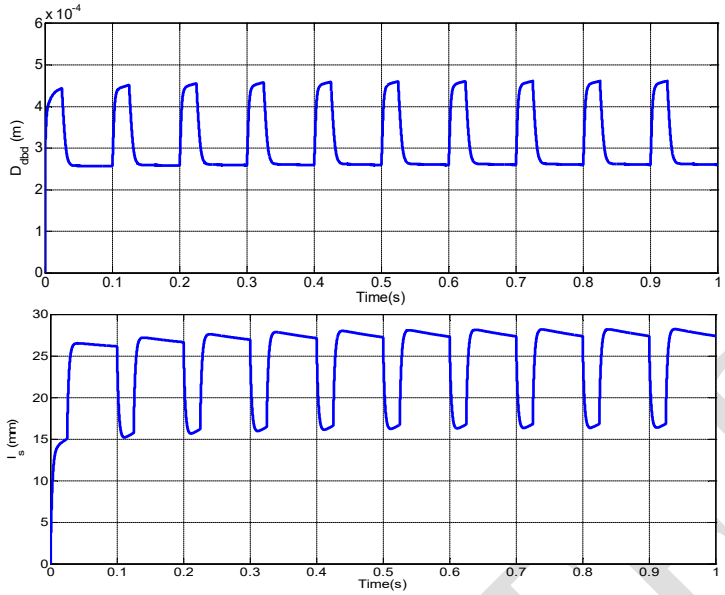

Figure 4. Dynamic response waveforms of the length of weld wire between the molten droplet and contact point (l_s), welding current (I_a), welding voltage (U_a), and droplet diameter (D_{dbd}).

3.2 *Discussion results*

Through the simulation results of Figure 3, the rectified current (Id) settled at value 100A in a very short time without oscillations caused by serial connectivity between two-level rectifiers. The first-phase current of Bus1 and Bus 2 oscillate between ±100A, their form is non-sinusoidal due to non-linear charge effects. The consumed length of weld wire between the molten droplet and contact point (ls) within one second is around 120mm to get 10 droplets of molten wire, where each droplet has a diameter of 0.45mm as shown in Figure 4. To achieve the condition of droplet detachment, in each detachment, the welding current (Ia) must increase by more than three times the nominal value (3*100A), and welding voltage (Ua) decreases by 18V.

4 Grid Network-GMAW system under faulty switches

4.1 Open-circuit fault of the Thyristor

To investigate the grid network-GMAW behavior, an open-circuit fault is induced in the switch S^1_{11}at time 0,5s, as indicated in Figures 5, 6, and 7.

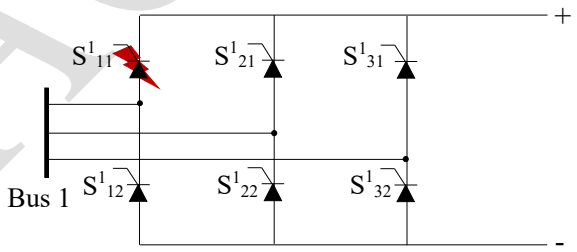

Figure 5. Two-level rectifier1 under the faulty S^1_{11} switch.

4.2 Simulation results and discussion

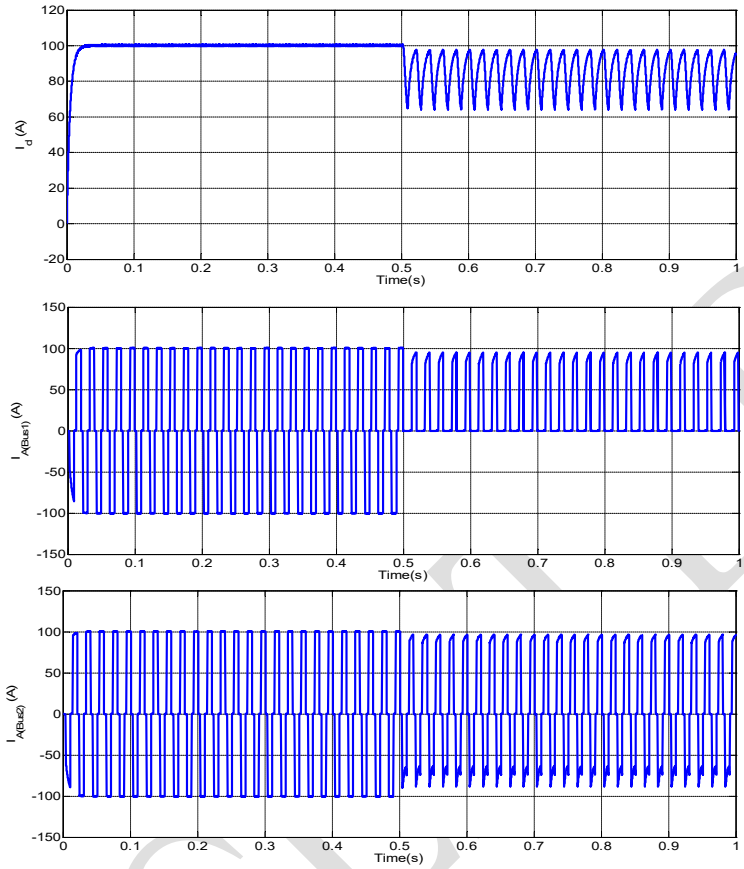

Figure 6. Simulation results of rectified current (I_d), current of the first phase of bus1(I_A(Bus1)), and current of the first phase of bus2(I_A(Bus2)) under the fault of switch opening S^1_{11} induced at 0.5s.

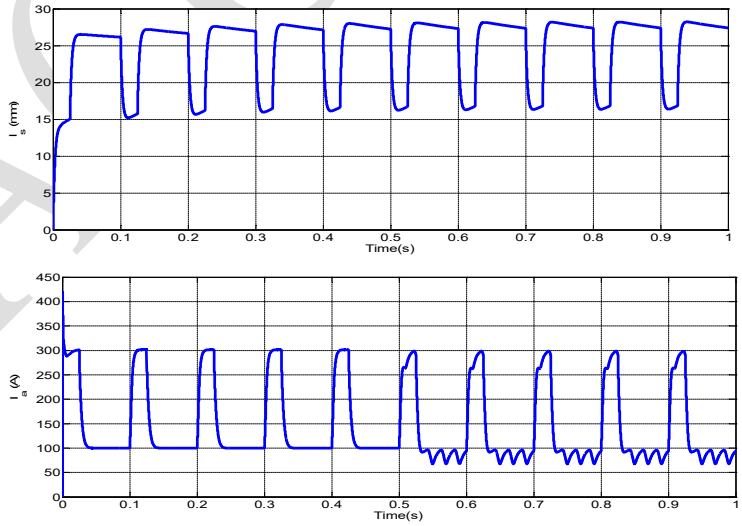

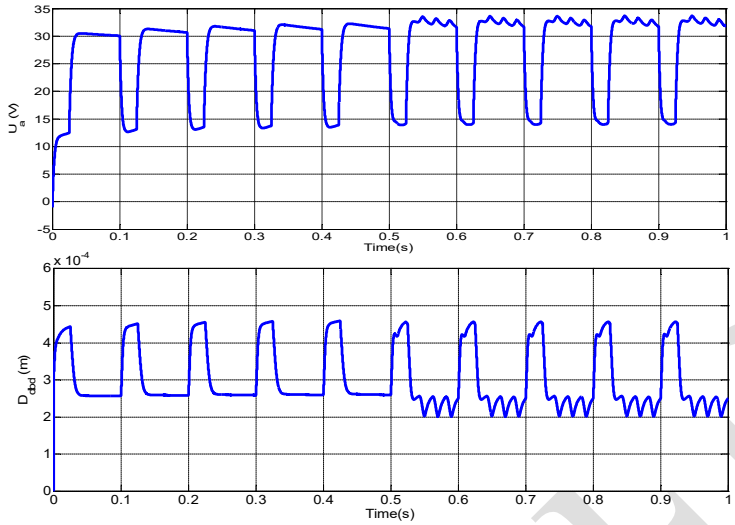

Figure 7. Dynamic response waveforms of the length of weld wire between the molten droplet and contact point (ls), welding current (Ia), welding voltage (Ua), and droplet diameter (D_{dbd}) under the fault of switch opening S^{1}_{11} induced at 0.5s.

After the fault concerning the current of the first phase of bus1, its wave decreases by 55% higher than the wave of the current of the first phase of bus2 which decreased by 23%, so it can be said that the fault occurred in the rectifier which is connected with bus1. For the arc current (I_a) that has three operations of current welding, the first is called the short-circuit, the second is called the detachment and the third is called the cooling as shown in Figure7. Immediately after the fault, the short-circuit and cooling operations do not take enough time during melting and cooling of the welding wire, the welding voltage (U_a) and form of the droplet are also affected which negatively affects the quality of welding. But the length of weld wire between the molten droplet and contact point (l_s) does not fully affect because it runs at a constant speed to feed the welding torch. The fault detection can be noticed easily, however, the faulty switches are localized only with the help of some diagnostic techniques.

5 Method detection and location of the open-circuit faults

This section concerns the well-known method of diagnosis of open-circuit faults applied to the two-level rectifiers which are considered an important part of the grid network-GMAW system. The adopted diagnostic technique in this study is based on Park's vectors method of the currents mean value.

5.1 *Fault detection by the mean value of the Park's vectors*

The advantage of a mean value of currents of the d-q axis during a cycle is a methodological principle of the Park vectors [24], Equation (8) represented the Park's transformation vector from three-phase currents into two currents of the d-q axis. Equation (17) calculated the mean values of currents d-q during a cycle. The magnitude and angle (argument) are calculated. Equation (20) can be expressed in a d-q system coordinates from the obtained two mean values of the currents.

$$\begin{cases} i_d = \frac{2}{3} i_a - \frac{1}{3}(i_b + i_c), i_q = \frac{1}{\sqrt{3}}(i_b - i_c) & (17) \\ \mu_x = \frac{1}{N}\sum_{K=1}^{N} i_x(k\tau) & (18) \\ \mu = \mu_d + j\mu_q = M_\mu \angle \theta_{\mu 2} & (19) \\ M_\mu = \sqrt{\mu_d^2 + \mu_q^2}, \theta_\mu = \tan^{-1}\frac{\mu_q}{\mu_d} & (20) \end{cases}$$

The mean value vector method can be applied to the three currents of bus1and bus2 under the healthy and faulty two-level rectifiers. An open-circuit fault in the Thyristor switch can produce disturbances in the rectified current (Id).
The diagnostic technique consists of calculating the mean values of the three currents of two buses [25] from these current values, a threshold band is proposed to detect the faults. Two threshold band limits are put to detect the open circuit faults of the Thyristors.

5.2 Simulation results and discussion

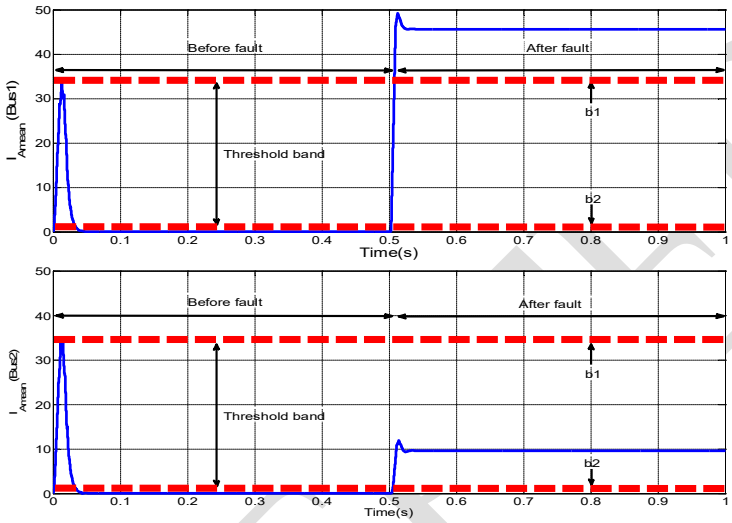

Figure 8. Simulation results of mean values of currents of the first phase of bus1 and bus2 under open-circuit fault induced in switch S^{1}_{11} and examined by threshold band limits.

Figure 8 shows the simulation results of the currents mean values with a limited threshold band to detect the open-circuit fault.

If the mean values of the three-phase currents I_A, I_B, and I_C are within the threshold band limits B, it means that there is no open-circuit fault.

If the currents mean values exceed the limits values (b_1 or b_2) of threshold band B, at this exact time, the fault can be determined.

5.3 Fault locating by the mean value of the Park's vectors

5.3.1 Simulation results and discussion

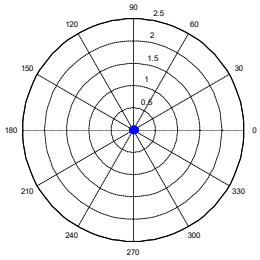

Figure 9. Fault angle θ_μ by the polar coordinates under a healthy state.

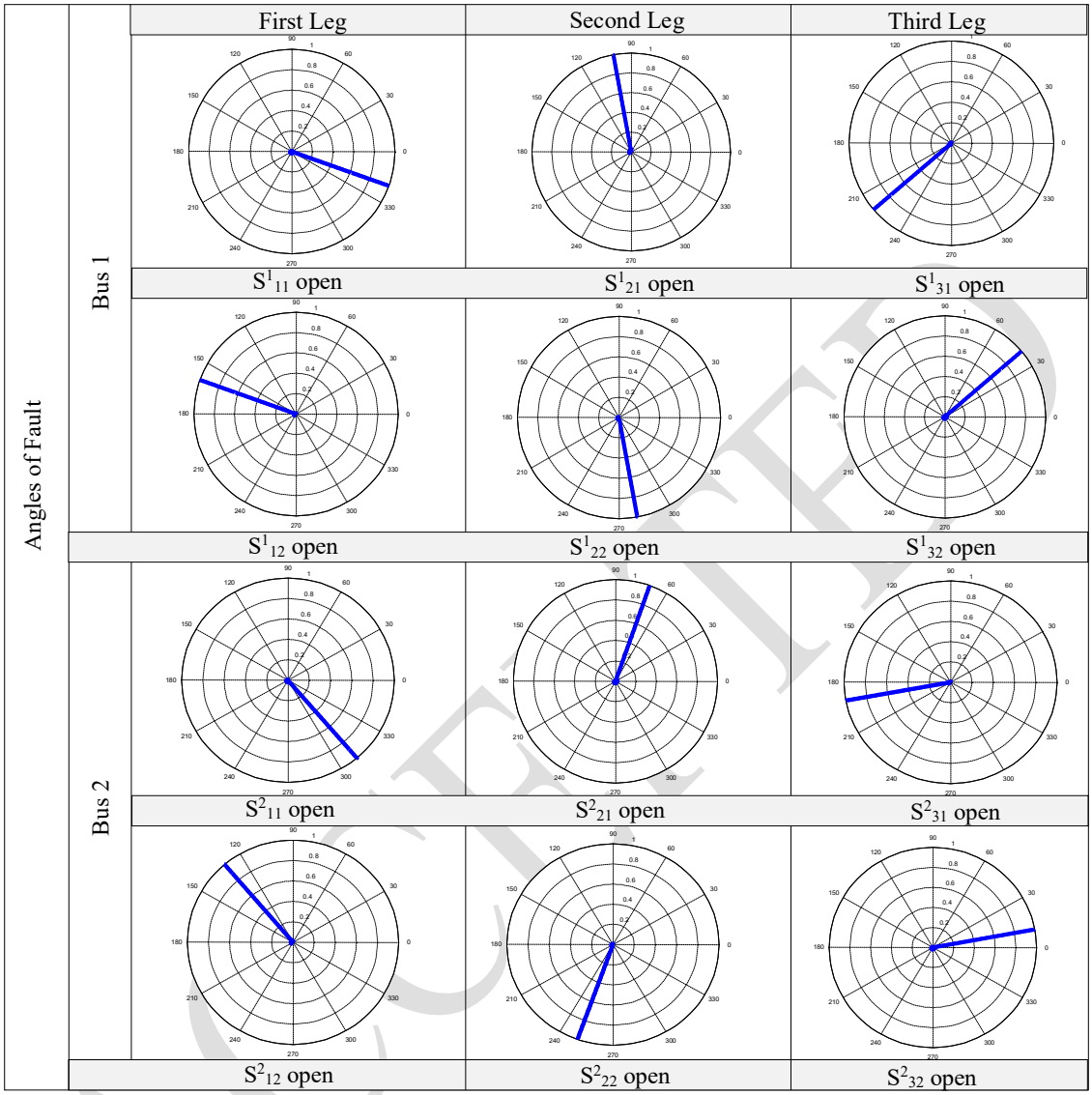

Figure 10. Graphical polar representation of the different rectifiers Thyristor switches faults by methods of captured currents.

The polar coordinates technique is applied to study the rectifier under faultless state, Figure 10 describes its fault angle position.

In the healthy state, the value of fault angle θμ is 0 which means that no open-circuit fault happens.

The polar coordinates technique is evaluated under the twelve faulty switches, each one is tested separately, an open circuit fault is induced at 0.5s, the proposed polar angle trajectories are represented in the different fault angle positions corresponding to each switch as shown in table 2 and Figure 10.

Figure10 represents the fault angles previously indicated in Table 2, they are obtained from the diagnostic technique by the polar coordinates method.

The flowchart of the different steps of the mean currents values of the Park's vectors method is shown in Figure13.

Through the determinations of the fault angles, it can be noted that the angles change with changing the captured currents of bus1 and bus2, which means the binary diagnostic method has been applied in two

rectifiers, each one has its fault angles, they are completely different in terms of the positioning, this is ensured by the polar coordinates technique that makes easy fault location.
So, it is possible to say that the diagnosis method is an important tool to locate the open circuit faults, but not sufficient to ensure the required quality of the welding process. For this purpose, it is advisable to integrate reconfigurable fault-tolerant rectifiers to ensure good welding quality. This is the main contribution of this study.

Table 2. Location of two rectifiers' open-circuit faults with corresponding fault angle intervals

Open Switch		Magnitude M_μ	Interval of θ_μ
Rectifier 1	S^1_{11}	Exceed threshold band limits	$300 < \theta_\mu < 0$
	S^1_{12}		$120 < \theta_\mu < 180$
	S^1_{21}		$60 < \theta_\mu < 120$
	S^1_{22}		$240 < \theta_\mu < 300$
	S^1_{31}		$180 < \theta_\mu < 240$
	S^1_{32}		$0 < \theta_\mu < 60$
Rectifier 2	S^2_{11}		$300 < \theta_\mu < 0$
	S^2_{12}		$120 < \theta_\mu < 180$
	S^2_{21}		$60 < \theta_\mu < 120$
	S^2_{22}		$240 < \theta_\mu < 300$
	S^2_{31}		$180 < \theta_\mu < 240$
	S^2_{32}		$0 < \theta_\mu < 60$

6 Reconfiguration of the faulty rectifier

6.1 Topology of reconfigurable fault-tolerant rectifier

According to Figure11, the redundant rescue leg is added to avoid any faulty leg by using the fast-acting fuses [26,27]. These fuses must have physical characteristics inferior to those of semiconductor switches. The different fault-tolerant two-level rectifiers can tolerate the following faults scenarios: short-circuit or open circuit of switches or open phase. However, the topology which is proposed in Figure 11 can tolerate open-circuit and/or short-circuit faults with a single reconfiguration.
The fourth leg is connected to the main legs through a set of TRIACS. Under the healthy case, the TRIACS disconnects the fourth leg. Immediately after the fault, the faulty leg is released by two fast-acting fuses, in addition at the same time, the TRIAC, connected to the faulty leg, connect to the fourth leg, thus, three healthy legs become connected to bus1 in this side, and the other side to accomplish the exploitation of reconfiguration.

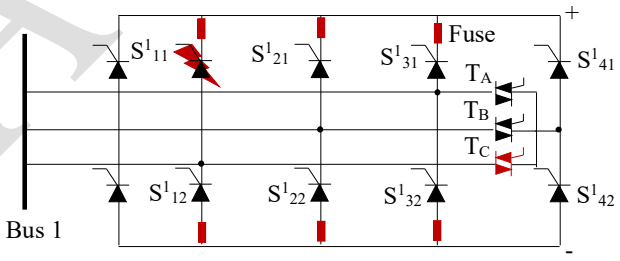

Figure 11. Reconfiguration of the two-level rectifier.

Figure 12 shows the general scheme of reconfigurable two-level fault-tolerant rectifiers with their diagnostic blocks. The latter ones are linked with the detection and location blocks of opened circuit fault. The decision

block starts immediately to send the reconfiguration commands to the reconfigurable rectifier. The detection, location, and reconfiguration processes depend on the current values (I_A, I_B, I_C) of bus1 and bus 2.

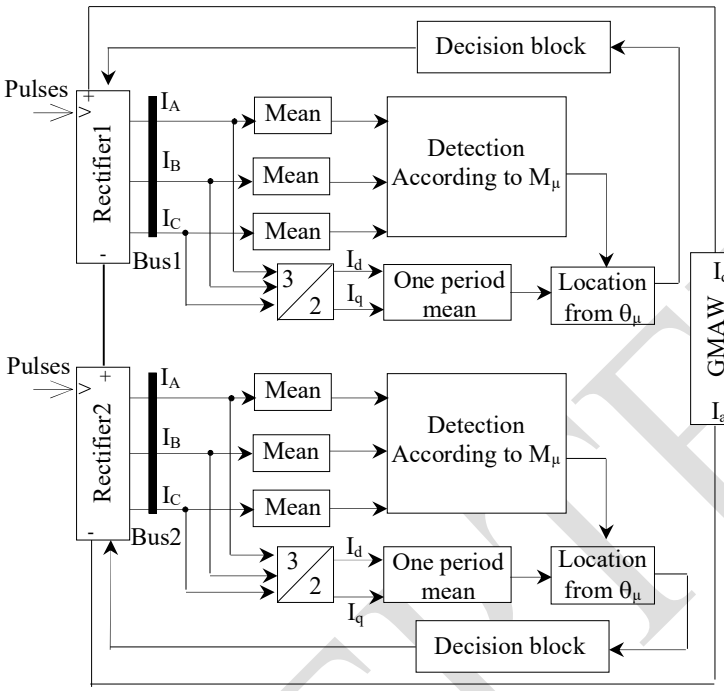

Figure 12. Three-phase rectifier fault-tolerant control scheme connected GMAW system with isolation capability.

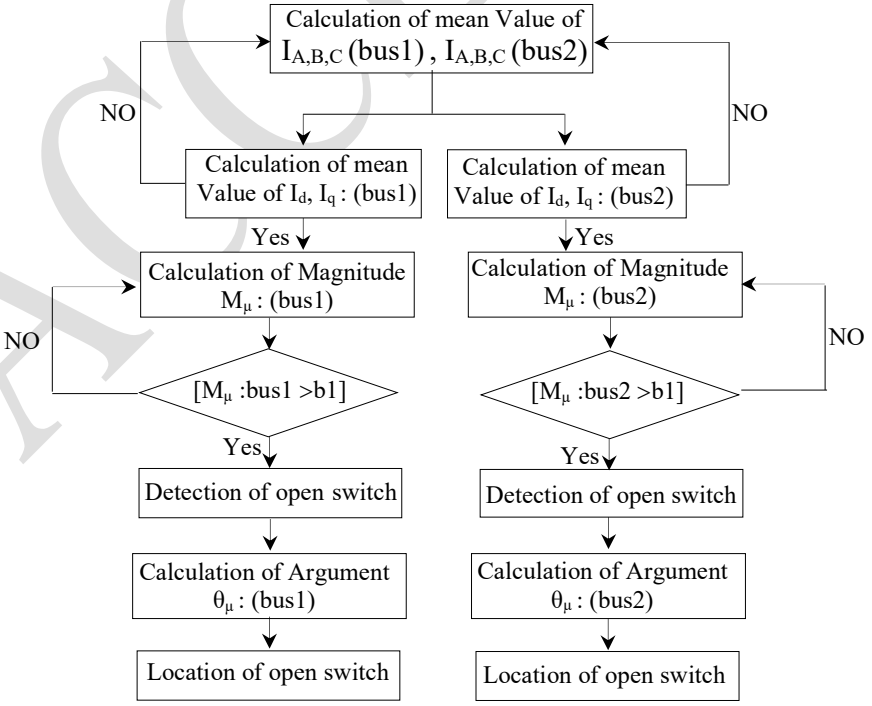

Figure 13. Flowchart of the mean value of the Park's vectors currents method.

6.2 Simulation results and discussion

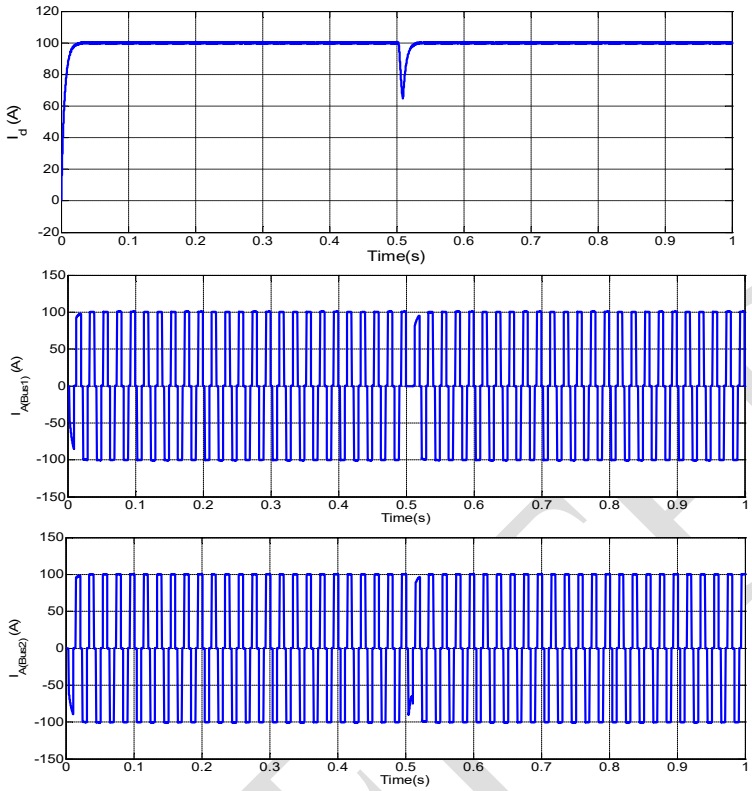

Figure 14. Simulation results of rectified current (I_d), current of the first phase of bus1(I_A(Bus1)), and current of the first phase of bus2(I_A(Bus2)) under the fault of switch opening S^1_{11} induced at 0.5s.

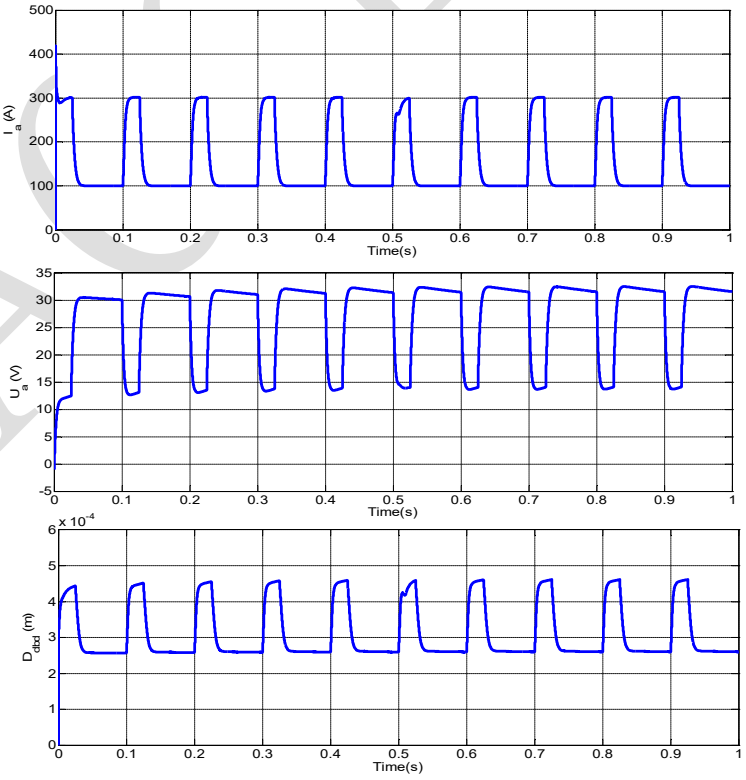

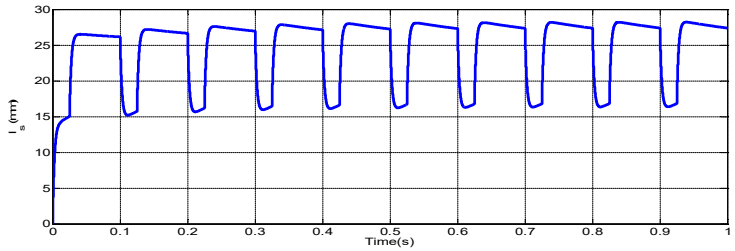

Figure15. Dynamic response waveforms of the length of weld wire between the molten droplet and contact point (l_s), welding current (I_a), welding voltage (U_a), and droplet diameter (D_{dbd}) under an open circuit fault of the switch S^1_{11} induced at 0.5s.

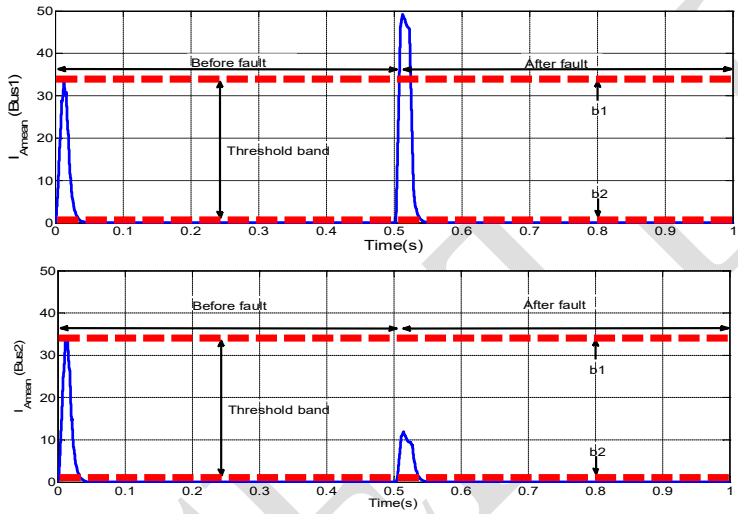

Figure 16. Simulation results of mean values of currents of the first phase of bus1 and bus2 under open-circuit fault induced in switch S^1_{11} and examined by threshold band limits.

The fault detection block depends on the calculation of magnitude Mμ of two buses according to their exceeding threshold band limits (Figure 8, and Table 2). The blocks of fault locations as a function of θ_μ depend on the mean values of the direct and quadratic currents of two buses (I_d, I_q) as mentioned in Figure 8.

The coming section aims to investigate the impact of the included fault-tolerant rectifiers on the buses' currents. Before inducing the fault, the rectified current (I_d) had a fixed value of 100A, whereas, when the open circuit fault occurs, the I_d decreases to 65A, by the help of the diagnosis technique and rectifiers reconfiguration, they make the restoration of the rectified current to its initial value, this leads to no negative effects on the results of buses currents, welding current, welding voltage, and droplet diameter. In Figure16, the current mean value of bus1 exceeds the upper limit of the threshold band, however, that of bus 2 stays within the limits; it means that the fault occurs only in bus 1 of the upper rectifier. After the reconfiguration of rectifier1, the current mean value of bus1 returns to the threshold band. As result, it can be said that the fault is disappeared. Figure17 presents the steps of location and isolation of the fault and reconfiguration of the rectifiers to be added to the flowchart of Figure 13 to ensure the process continuity of the entire system.

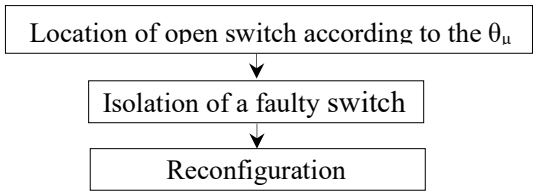

Figure 17. Flowchart of the isolation of the fault and reconfiguration steps of the fault tolerant rectifier.

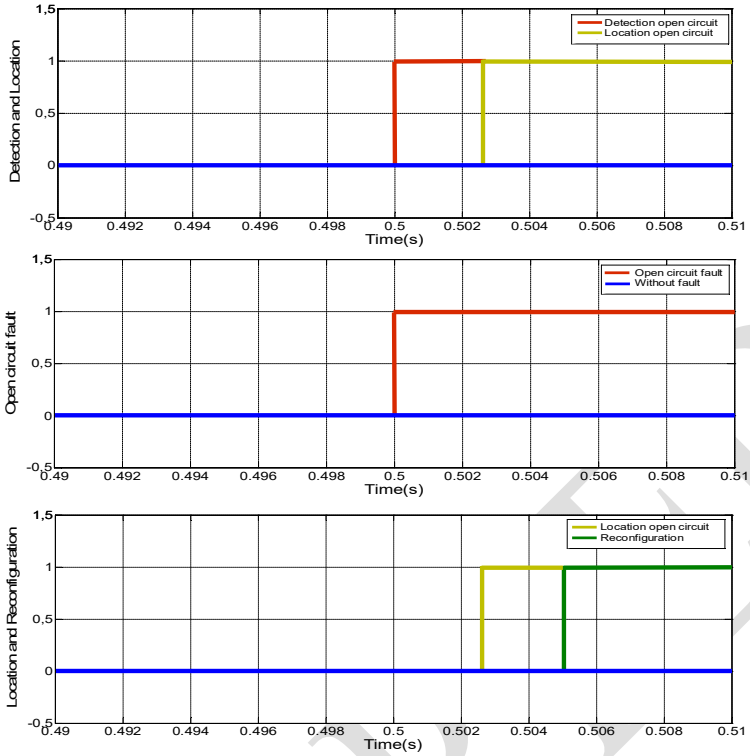

Figure 18. Timeline of the healthy operation, the fault duration, and the post-fault operation of open-circuit fault introduced at Thyristor switch S^{1}_{11} of the rectifier1.

Figure 18 illustrates the timeline before and after the fault inclusion, it can be noticed that all operations of detection, location, and reconfiguration have lasted 0.005s. This lap of time is highly sufficient to guarantee the continuity of the GMAW system.

7 Real-time processor-in-the-loop implementation

The performance of the proposed GMAW process is confirmed experimentally through a setup based on the dSPACE ds1103 panel. According to Figure 19, the processor in-the-loop (PIL) setup consists of an independent control processing unit (CPU), a real-time simulator, a communication channel, and a personal computer (PC) for monitoring the experimental results.

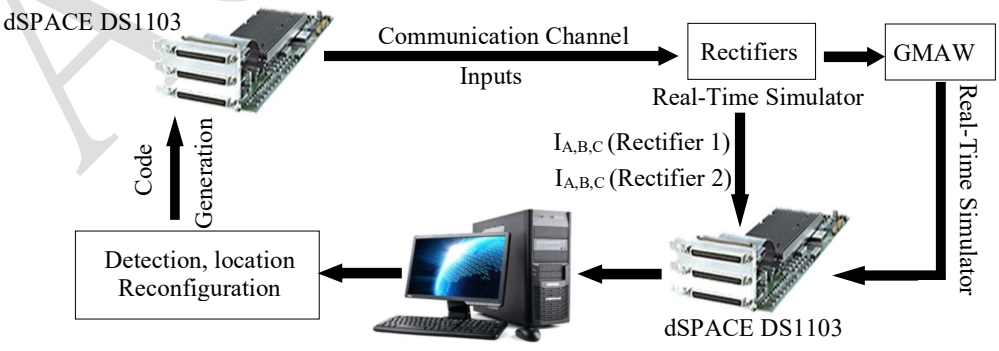

Figure 19. Experimental scheme set up for diagnostic and reconfiguration for the GMAW process.

The real-time simulator sends the state variables to the CPU through channel communication at each sampling time. Therefore, the CPU computes the optimal control action and sends it to the real-time simulator [28]. The purpose of Figure 20 is to prepare and download the generated code of a diagnostic (detection, location) and reconfiguration algorithm for the two fault-tolerant rectifier, in addition to examination of the proposed diagnostic technique through the processor-in-the-loop for the experimental setup and testing the numerical equivalence of the proposed diagnostic technique and the generated code.
The generated code is responsible for controlling the reconfigurable fault-tolerant rectifier, sending the pulses to the TRIACs and Thyristors and isolating the faulty leg.
In Figure 20, the power converter, diagnostic and reconfiguration blocks are located in the simulation model to generate the diagnostic and reconfiguration code.

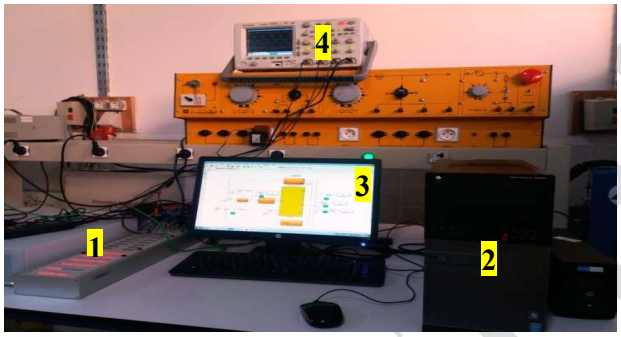

(1) : dSPACE DS1103(CPU)
(2) : PC
(3) : Simulation model:
(Rectifiers, GMAW, Diagnosis, Reconfiguration)
(4) : Oscilloscope

Figure 20. Examining the proposed diagnostic technique through the processor-in-the-loop for the experimental setup.

The parameters of the GMAW system and control scheme, used in PIL implementation tests, are the same as those used in the simulation. The captured waveforms are recorded using an AGILENT TECHNOLOGIES oscilloscope.

7.1 Captured signals and discussion

Figure 21, Figure 22, Figure 23, Figure 24, and Figure 25 show the experimental waveforms of the length of weld wire between the molten droplet and contact point, welding current, welding voltage, droplet diameter, current of the first phase of bus1 and mean value current of Bus1 under the healthy and faulty states. All of these results are similar to simulation results obtained previously. Thus, it confirms the reliability of the reconfiguration fault-tolerant rectifiers applied to the GMAW process connected to the electric network.

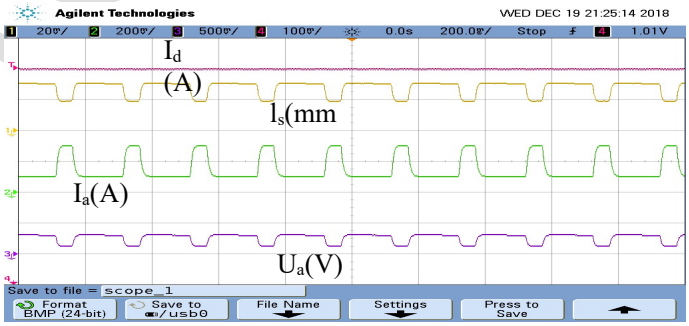

Figure 21. Captured waveforms of the rectified current (I_d), length of weld wire (l_s), welding current (I_a), and welding voltage (U_a) under the healthy state.

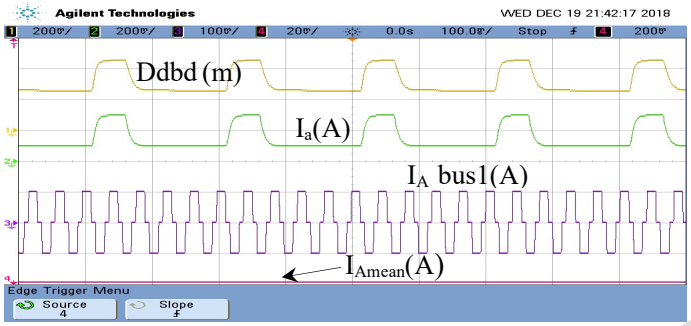

Figure 22. Captured waveforms of droplet diameter (D_{dbd}), welding current (I_a), current of the first phase of bus1(I_A Bus1), and mean value of (I_A Bus1) under the healthy state.

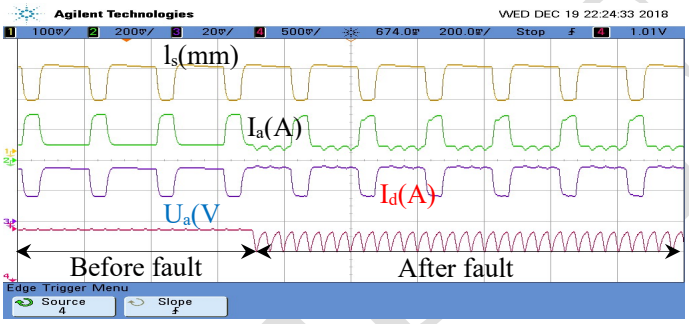

Figure 23. Captured waveforms of the length of weld wire (l_s), welding current (I_a), welding voltage (U_a), and rectified current (I_d) under two states healthy and failing (open-circuit).

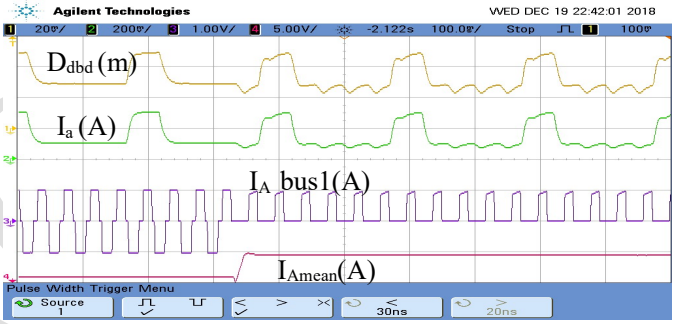

Figure 24. Captured waveforms of droplet diameter (D_{dbd}), welding current (I_a), current of the first phase of bus1(I_A Bus1), and mean value of (I_A Bus1) under two states healthy and failing (open-circuit).

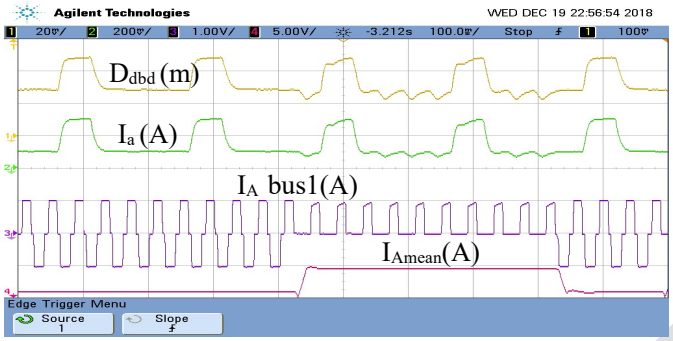

Figure 25. Captured waveforms of droplet diameter (D_{dbd}), welding current (I_a), current of the first phase of bus1(I_A Bus1), and mean value of (I_A Bus1) of the healthy operation, the fault duration, and the post-fault operation of open-circuit fault.

8 Conclusion

This paper focuses first on the advantages of connecting between the electrical network, two rectifiers, and the Gas Metal Arc Welding process (GMAW) and the possibility of using this connection in industrial applications.

In the case where the faults (open circuit and/or short circuit) occur in any rectifier, these can have some negative effects on both the grid network and the GMAW process.

At the level of the GMAW process, the faults affect the performance of dynamic response waveforms by inducing perturbations and distortion of the current and voltage of welding, and the deformation of droplet diameter, which leads to bad welding quality of the workpiece.

Second, to bypass all mentioned defects, the diagnosis technique, related to the detection and location of the faulty switch (Thyristor) under open circuit, gives very acceptable results in terms of early detection and the precise fault location; the mean values of the Park's vector method are combined with polar coordinates to locate the faulty switches with clear graphical illustrations. The different obtained results are presented to illustrate the dynamic and electrical responses. Both of them can give a good diagnosis of healthy and faulty rectifiers.

Third, the inclusion of the fault-tolerant rectifiers in series between the grid network and the GMAW process can overcome the rectified current oscillations under open-circuit fault.

The very short time of 0,005s, taken by the detection, location, and reconfiguration operations, is highly sufficient to ensure the right diagnosis and good service continuity of the electrical grid network and the GMAW system.

The signals captured by the processor in the loop prove the success of the proposed diagnostic technique and complete the generation of the code to be sent to the target converter in a subsequent new process called hardware in the loop.

For prospects, it would be better to apply the diagnosis technique based on multi-level rectifiers. This will be the scope of a future paper.

Acknowledgment

This work was supported by the Research Center in Industrial Technologies CRTI, P.O.Box 64, Cheraga 16014 Algiers, Algeria.

References

[1] P. K. Ghosh, Introduction to Gas Metal Arc Welding Process, Pulse Current Gas Metal Arc Welding (Springer, Singapore, 2017), pp. 1–30.
[2] P. Kah, R. Suoranta, J. Martikainen, " Advanced gas metal arc welding processes, " Int J Adv Manuf Technol 67 655–674, 2013.
[3] Y. Xu, et al., " Welding seam tracking in robotic gas metal arc welding," Journal of Materials Processing Technology 248, 18-30, 2017.
[4] M. Vijeh, M. Rezanejad, E, Samadaei, K. Bertilsson, " A general review of multilevel inverters based on main submodules: Structural point of view, " IEEE Transactions on Power Electronics, 34, no 10, p. 9479-9502, 2019.
[5] B. Wu, High-Power Converters and AC Drives. Hoboken, NJ: Wiley, 2006.
[6] O.F.Benaouda, A.Bendiabdellah, B. Cherif, "Contribution to Reconfigured Multi-Level Inverter Fed Double Stator Induction Machine DTC-SVM," International Review on Modelling and Simulations (IREMOS)., vol. 9, no. 5, pp.1-13. Sep 2016.
[7] B. Wang, J. Wang, A. Griffo, B. Sen, " Stator turn fault detection by second harmonic in instantaneous power for a triple-redundant fault-tolerant PM drive," IEEE Transactions on Industrial Electronics, 65(9), 7279-7289, 2018.
[8] A.M.S. Mendes, M.B. Abadi, S.M.A. Cruz, " Fault diagnostic algorithm for three-level neutral point clamped AC motor drives, based on the average current Park's vector, " IET Power Electronics, 7(5), 1127-1137,2013.
[9] S. Abramik, W. Sleszynski, J. Nieznanski, H. Piquet, "A Diagnostic Method for On-Line Fault Detection and Localization in VSI-Fed AC Drives," EPE 2003, 10th European Conference on Power Electronics and Applications,Toulouse, France. CD-ROM paper.
[10] R. Peuget, S. Courtine, J.P. Rognon, "Fault Detection and Isolation on a PWM Inverter by Knowledge-Based Model, " IEEE Transactions on Industry Applications, vol. 34, No. 6, pp. 1318-1325, 1998.
[11] B. Lu and S. K. Sharma, "A literature review of IGBT fault diagnostic and protection methods for power inverters," IEEE Trans. Ind. Appl, Vol. 45, No. 5, pp.1770-1777, Sep./Oct. 2009.
[12] B. Lu and S. K. Sharma, "A survey of IGBT fault diagnostic methods for three-phase power inverters," 2008 International Conference on Condition Monitoring and Diagnosis, pp.1-8, Oct. 2008.
[13] B. Li, S. Shi, B. Wang, G. Wang, W. Wang, D. Xu, " Fault diagnosis and tolerant control of single IGBT open-circuit failure in modular multilevel converters," IEEE Transactions on Power Electronics, 31(4), 3165-3176, 2015.
[14] F. W. Fuchs, "Some diagnosis methods for voltage source inverters in variable speed drives with induction machines-A survey," in Proc. IEEE Ind. Conf., pp.1378-1385, 2003.
[15] J. Mavier, F. Richardeau, H. Piquet, "Onduleur Reconfigurable, à Tolérance de Pannes, pour l'Alimentation d'un Moteur Triphasé Synchrone à Aimants Permanents, et Ensemble Desdits Onduleur et Moteur, " Aux noms de Airbus France SAS, Centre National de Recherche Scientifique, Institut National Polytechnique de Toulouse, FR 2 892 243 B, 2010.
[16] L. Boulon, D. Hissel, A. Bouscayrol, O. Pape, M.-C. Péra, "Simulation Model of a Military HEV With a Highly Redundant Architecture, " IEEE Transactions on Vehicular Technology, Vol. 59, No. 6, pp. 2654-2663, 2010.
[17] B. Mvola, P. Kah, & P. Layus, "Review of current waveform control effects on weld geometry in gas metal arc welding process," Int J Adv Manuf Technol 96, 4243–4265, 2018.
[18] N. Arif, J.H Lee, C.D Yoo, " Modeling of globular transfer considering momentum flux in GMAW, " Journal of Physics D (Applied Physics) 41:1–6. 2008.
[19] J. C. Amson, "Lorentz force in the molten tip of an arc electrode, ", British Journal of Applied Physics, vol. 16, pp. 1169–1179.1965.
[20] A. M. Mousavi and M. Haeri, "Estimation and control of droplet size and frequency in projected spray mode of a gas metal arc welding (GMAW) process," ISA Transactions 53(3):408–417.2011.
[21] P. Hu, J. Huang, M. Zeng, "Application of fuzzy control method in gas metal arc welding, " Int J Adv Manuf Technol 92, 1769–1775, 2017.
[22] P. J. D. D. O.Evald, J. L.Mor , R. Z. Azzolin, S. S. D. C. Botelho, "A nonlinear coupled-variables model for mass transfer modes in MIG-MAG processes with experimental validation, " International Journal of Modelling, Identification and Control, 31(4), 361-373, 2019.

[23] S. Soltani, M.Eghtesad, , Y. Bazargan-Lari, "Mass and heat transfer control in the GMAW process utilizing feedback linearization and sliding mode observer, " International Communications in Heat and Mass Transfer, 111, 104410, 2020.
[24] R. Peuget and S. Courtine, " Diagnosis methods for IGBT open switch fault applied to 3-phase AC/DC PMW converter," IEEE Trans. on Ind. Appl., Vol.12,No.1, pp.120-127, January.2012.
[25] J. Fernando Silva, Sónia F. Pinto, "Control Methods for Switching Power Converters (ed)," chapter 34, pp. 935-998;
[26] R. L. de A. Ribeiro, C. B. Jacobina, E. R. C. da Silva, and A. M. N. Lima, "Fault-tolerant voltage-fed PWM inverter ac motor drive systems," IEEE Trans. Ind. Electron., vol. 51, no. 2, pp. 439 – 446, Apr. 2004.
[27] B.A. Welchko, T.A. Lipo, T.M. Jahns, and S.E. Schulz, "Fault tolerant three-phase AC motor drive topologies: a comparison of features, cost, and limitations," IEEE Trans. Power Electron., vol. 19, no. 4, pp. 1108 – 1116, July 2004.
[28] YH Chien, WY Wang, YG Leu, TT Lee, " Robust adaptive controller design for a class of uncertain nonlinear systems using online T–S fuzzy-neural modeling approach, " IEEE Transactions on Systems, Man, and Cybernetics, Part B (Cybernetics); 41(2):542-552, Apr 2011.